IEEE Access
Multidisciplinary | Rapid Review | Open Access Journal

Received 8 April 2024, accepted 18 April 2024, date of publication 24 April 2024, date of current version 1 May 2024.

Digital Object Identifier 10.1109/ACCESS.2024.3393409

APPLIED RESEARCH

Integrated Thermal Management of Electric Vehicles Based on Model Predictive Control With Approximated Value Function

YOUYI CHEN[1], KYOUNG HYUN KWAK[1], JAEWOONG KIM[2], DEWEY DOHOY JUNG[1], AND YOUNGKI KIM[1], (Senior Member, IEEE)
[1]Mechanical Engineering, University of Michigan–Dearborn, Dearborn, MI 48128, USA
[2]Hyundai-Kia Motor Company, Hwaseong-si, Gyeonggi-do 18280, South Korea

Corresponding author: Youngki Kim (youngki@umich.edu)

The work of Youyi Chen, Kyoung Hyun Kwak, Dewey Dohoy Jung, and Youngki Kim was supported by Hyundai-Kia Motor Company.

ABSTRACT The thermal management system (TMS) in electric vehicles (EVs), including climate control and battery thermal regulation, consumes more energy than any other auxiliary components. Therefore, optimizing TMS control is crucial for enhancing EV driving range. However, the complexity of the TMS, described by a differential algebraic system, poses challenges for real-time optimal control. This study proposes model predictive control (MPC)-based solutions for integrated TMS operation in EVs. An optimal thermal management problem is formulated using economic nonlinear MPC (NMPC), and its performance is evaluated. To reduce computational load, an approximated value function (VF) is introduced based on the economic NMPC results. A linear-time-varying MPC (LTV-MPC) with the approximated VF is proposed for real-time implementation using quadratic programming, and through simulations it is compared with the baseline NMPC controller and a rule-based (RB) controller. Results reveal that the LTV-MPC with an approximated VF performs similarly to NMPC while offering slightly compromised cooling performance. It also significantly reduces the computational time by a factor of 10^4 compared with NMPC owing to the short prediction horizon enabled by the approximated VF. Furthermore, when compared with the RB controller, the proposed LTV-MPC achieves energy savings in the range of 22.3% to 29.8%.

INDEX TERMS Electric vehicle, thermal management, model predictive control, heating, ventilation, air-conditioning control.

NOMENCLATURE

SYMBOLS

$\Delta\omega$	Absolute humidity difference (inlet - outlet).
$\dot{m}$	Mass flow rate [kg/s].
$\dot{Q}$	Heat transfer rate [W].
ϵ	Heat exchanger effectiveness.
$\hat{V}$	Approximated Value function.
ω	Weighing factor.
τ	Time constant.
A	Surface area [m^2].
C	Heat capacity [J/K].
c_p	Specific heat capacity [J/kg-K].
D_h	Hydraulic diameter of coolant channel [m].
h	Specific enthalpy [J/kg].
I_{bat}	Battery current [A].
J	Cost function.
k_c	Thermal conductivity [W/m-K].
k_{door}	Ratio of the air mass flow rate of inner condenser to the total flow rate.
L	Stage cost function.
m	Mass [kg].
N_p	Number of prediction steps.
Nu	Nusselt number.
P_{bat}	Battery power [W].
R_{bat}	Internal resistance [Ω].

The associate editor coordinating the review of this manuscript and approving it for publication was Jiajie Fan.

T	Temperature [°C].
t	Time [s].
U	Overall heat transfer coefficient [W/m^2-K].
U_{oc}, U_{bat}	Open circuit voltage, terminal voltage [V].
V	Value function.
v_{veh}	Vehicle speed [km/h].
x, u, d	State, control, disturbance.

SUBSCRIPTS/SUPERSCRIPTS

a, c, r	Air, coolant, refrigerant.
amb	Ambient.
bat	Battery.
blwr	Blower.
cab	Cabin air.
chlr	Chiller.
comp	Compressor.
cond, c	Condenser.
ewp	Electric water pump.
evap, e	Evaporator.
fan	Fan.
htr	Electric heater.
in, *out*	Inlet, outlet.
ic	Inner condenser.
int	Interior.
lb, *ub*	Lower bound, upper bound.
solar	Solar heat load.
str	Cabin structure.

I. INTRODUCTION

A. BACKGROUND

The market share of electric vehicles (EVs) has been growing rapidly during the past five years and is projected to be up to 25% in 2030, according to a report by the International Energy Agency (IEA) [1]. Although EVs are nowadays familiar to and accepted by customers, the driving range remains one of the concerns for EV buyers [2]. As pointed out by Khoury and Clodic [3], the thermal management system (TMS) of EVs, including the heating, ventilation, and air-conditioning (HVAC) system and the battery TMS, accounts for the most significant energy consumption among all auxiliary components. According to a study by Bellocchi et al. [4], the energy consumed by the HVAC system can decrease the driving range of EVs by up to 30–40%, especially in hot weather conditions. On the other hand, the efficiency and lifespan of the battery system are highly dependent on the operating temperature, with the ideal range being around 25–40 °C [5].

Depending on the type of EV, the battery TMS has various configurations, including air-based and liquid-based types [6]. With the increasing size of modern EV batteries, a liquid-based battery TMS becomes necessary to provide much higher heat capacity and thermal conductivity. Compared with an air-based battery TMS, a liquid-based battery TMS can be up to 3500 times more efficient [6]. However, a liquid-based structure is more complicated, especially when the thermal dynamics of a liquid coolant are coupled with the refrigerant circuit of an HVAC system. Considering the high energy consumption of the HVAC system, the temperature sensitivity of the battery system, and the highly coupled thermal dynamics between them, it is essential to develop energy-efficient management strategies that consider both the HVAC and battery cooling systems. This holistic approach is crucial for achieving optimal vehicle thermal management and maximizing driving range performance.

On the other hand, model predictive control (MPC) has been gaining popularity for EV controllers, especially with the advancement of connected and autonomous vehicle (CAV) technology enabled by vehicle-to-infrastructure (V2I) and vehicle-to-vehicle (V2V) communications [7], [8]. With these communications, the ego vehicle is aware of the driving environment and the travel plans of other vehicles on the road. Taking that information into consideration, the ego vehicle can decide its optimal travel plan, including the speed profile and energy management. Therefore, the speed profile and the corresponding thermal load of the EV TMS can be predicted with decent accuracy, which makes predictive control algorithms realistic. Economic MPC has especially been drawing much attention for the energy-efficient optimal control of thermal systems [9], [10], [11]. In the operation of an economic MPC controller for a thermal system, optimal control is achieved by minimizing an economic or performance cost by exploring states and controls within a prediction horizon, where the cost function evaluates energy consumption and thermal regulation. Considering the various driving conditions and the corresponding varying thermal management demands, it is necessary to have a real-time-implementable optimal control methodology for the EV TMS. However, performing such an optimization process in real time is still challenging, especially for the highly nonlinear EV TMS. Therefore, adequately reducing the computational cost of the MPC algorithms is essential.

B. LITERATURE REVIEW

Several studies have proposed approaches to reducing the computational burden of MPC algorithms for vehicle thermal management applications. Some of them focused on the HVAC system. Wang et al. [12], [13] developed a nonlinear model predictive control (NMPC) algorithm for vehicle thermal management by utilizing setpoints of the A/C system as control inputs. The algorithm is based on a phenomenological model and serves as a high-level controller to determine the control settings of the HVAC control panel. However, the algorithm does not account for the optimal control of the refrigerant cycle components. Glos et al. [14] proposed an NMPC for an EV HVAC system. In their MPC algorithm, the heat transfer rate from the refrigerant cycle is considered as a control input, which significantly reduces the computational load as it avoids the need to compute the two-phase flow heat transfer. However, similar to the controllers mentioned earlier [12], [13], this NMPC has a

limitation in that it does not optimize the control of individual A/C components such as the compressor and the fan. Kibalama et al. [15] developed an NMPC controller for the HVAC system of EVs that reduces the computational demand by neglecting the cabin model. The refrigerant circuit is modeled by refrigerant pressures only, and the computational burden is further reduced by shortening the prediction horizon with an approximated value function. While these MPC approaches effectively reduce the computational cost, it is important to note that they focus solely on the HVAC system and do not consider other components of the vehicle thermal management system.

Indeed, the MPC methodology has been applied to liquid-cooled battery TMS as well. Lopez-Sanz et al. [16] developed an NMPC algorithm for battery thermal management based on a comprehensive physical model of the system. However, solving the nonlinear optimal control problem with ten state variables is computationally demanding and not suitable for real-time applications. Zhu et al. [17] developed an iterative algorithm that combines dynamic programming (DP) and MPC for an EV battery TMS. This algorithm considers the cooling of the battery using both cold air and liquid coolant. The control inputs in this approach are the inlet air and coolant temperature set-points, which require other control algorithms for regulation. Park and Ahn [18] developed a stochastic MPC for an EV battery TMS. In this controller, the refrigerant dynamics are determined by the compressor only, while the impact of the condenser fan is neglected. Consequently, the operational range of the refrigerant system is constrained within the prediction horizon of the MPC. Piao et al. [19] proposed a hierarchical MPC approach for an EV battery TMS. The algorithm uses the rate of heat transfer by the refrigerant system as the sole control variable while neglecting the refrigerant dynamics. Thus, additional control algorithms are required for regulating individual components. It is important to note that these studies have not considered the coupling between the HVAC and battery TMS, which is a crucial aspect to consider in the development of a comprehensive control strategy.

Compared with real-time MPC algorithms that focus solely on either HVAC systems or battery TMS, there are fewer published works on applications involving the integration of both systems. Glos et al. [20] developed a hybrid MPC approach for an EV TMS. For simplicity, the refrigerant system was simplified to a coefficient of performance model that considers the refrigerant temperature. However, the overall system remains complicated and the developed MPC algorithm focuses on mode selection only. In the work by Zhao et al. [21], a real-time hierarchical MPC approach is proposed for an integrated TMS that includes an HVAC system and an air-based battery TMS. Despite the hierarchical structure of the controller, the lower-level controller still uses setpoints of the A/C system as control inputs. Consequently, additional controllers are required to regulate the fan and compressor operations. Furthermore, the air-cooled battery cooling structure is designed for hybrid electric vehicles (HEVs) with relatively small battery sizes. As mentioned earlier, this type of cooling system may not be sufficient for battery EVs that have large battery packs. Amini et al. [22] developed a real-time hierarchical MPC approach for an integrated TMS that includes an HVAC system and an air-liquid-based battery TMS. Similar to the work by Zhao et al. [21], this approach uses setpoints of the A/C system as control inputs and incorporates the overall heat rejection rate of the battery TMS as an additional control input. It should be noted that when controlling components based on temperature or energy levels in a hierarchical manner, additional controllers are needed, potentially resulting in compromised optimality.

Considering the complexity of an integrated EV TMS, an NMPC controller with a reduced model can still be computationally expensive for real-time applications. Besides model reduction, several techniques have been studied in the literature for faster computations. One technique is using linear MPC with a quadratic cost function, which can accelerate the computation through quadratic programming (QP), as many fast QP solvers have been developed for online implementation [23], [24]. Typically, a highly nonlinear vehicle TM model is converted into a linear model via linearization around a fixed point [25], [26], [27], [28]. In HVAC applications, linear MPCs show comparable temperature tracking and energy-saving performance against NMPCs, while reducing computational time by up to 10 to 15 times [25]. However, in the previously published studies [25], [26], [27], [28], linearized models remain the same within the prediction horizon, referred to as linear-time-invariant (LTI) MPC. In transient cases where state and control trajectories vary significantly, the prediction accuracy can be compromised [29]. Therefore, a linear-time-varying (LTV) MPC based on successive online linearizations within the prediction horizon can be used to enhance the quality of the prediction and the performance of QP-based algorithms. To the best of the authors' knowledge, there have been relatively few applications of LTV-MPC in the field of TMS, especially when considering complex refrigerant circuits and their physics. In our previous work, we demonstrated the efficacy of physics-based modeling of various EV TMS problems utilizing an ideal vapor compression cycle in both NMPC and LTV-MPC [30], [31], [32]. In [33] we expanded these works and developed a physics-based control-oriented model of HVAC and battery cooling systems.

Besides linearization, the approximation of a cost-to-go function has been proven effective in accelerating MPC computation. In the studies by Park and Ahn [18] and Kibalama et al. [15], the cost-to-go values obtained from the DP solutions are approximated to a data-driven function of state variables and disturbances, which allows for a significant reduction in the prediction horizon. However, this approach is applied to HVAC-only systems or battery-only

systems and remains to be validated in more complicated integrated TMS applications.

C. RESEARCH SCOPE AND CONTRIBUTIONS

Summarizing the aforementioned literature, real-time energy-efficient thermal management for an integrated EV TMS remains a challenge, and the existing literature has the following two limitations: (i) there is a lack of a controller design considering both an HVAC system and a liquid-based battery cooling system; (ii) the thermal dynamics of the refrigerant system, especially of the two-phase heat exchangers, are typically omitted. To tackle this challenge, this paper proposes MPC-based control approaches, including an NMPC and an LTV-MPC with an approximated value function. Particularly, the integrated system encompasses an HVAC system and a liquid-based battery TMS, and these control approaches are designed to minimize the energy consumption of the integrated TMS while simultaneously regulating the battery temperature and the evaporator outlet air temperature. The main contribution of this paper is twofold:

1) An economic NMPC controller and a QP-based LTV-MPC controller are proposed based on the nonlinear physics-based EV TMS model developed in our previous work [33].
2) An approximated value function is developed based on the calibrated economic NMPC and implemented in the LTV-MPC controller, allowing for the use of a short prediction horizon, which leads to a significant reduction in computation.

D. OUTLINE OF SUBSEQUENT SECTIONS

The rest of the paper is organized as follows: Section II details the modeling of the integrated thermal management system of the considered EV. Section III presents the development of the economic NMPC and LTV-MPC controllers, including the development of the cost function and constraints as well as the tuning weights. In addition, the development of the approximated value function is provided in this section. Section IV discusses the comparison of the simulation results between the long-horizon economic NMPC, the short-horizon LTV-MPC, and the RB controller under three different driving cycles. Finally, concluding remarks and discussion on future directions are given in Section V.

II. THERMAL MANAGEMENT SYSTEM MODELING

This section presents the modeling approaches used to capture the dynamic behavior of the integrated TMS, which is adopted from our previous work [33], for the purpose of MPC design. The EV considered in this study is equipped with a 150 kW traction motor and a 64 kWh Li-ion battery pack. Figure 1 illustrates the schematic diagram of the integrated TMS, consisting of a refrigerant circuit and a battery coolant circuit. The system includes four heat exchangers: an evaporator, an inner condenser, an outdoor condenser, and a battery chiller. This TMS enables a battery

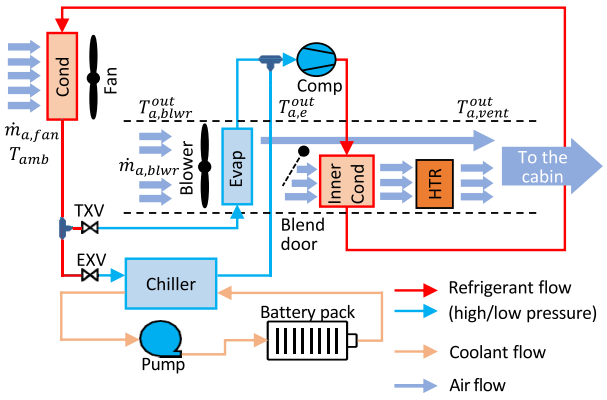

FIGURE 1. A schematic diagram of the considered thermal management system.

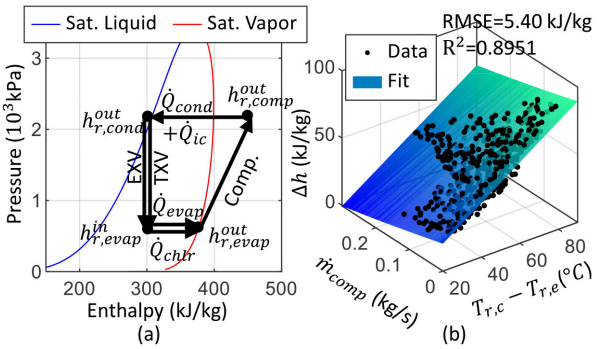

FIGURE 2. (a) Ideal vapor-compression cycle and (b) Δh_{comp} regression.

cooling mode, a cabin cooling mode with reheating,[1] and a heat pump mode in cold weather conditions [34]. In this specific refrigerant circuit structure, the inner condenser and the outdoor condenser are arranged in series, while the battery chiller and the evaporator are arranged in parallel. For this study, the focus lies on a scenario where the TMS performs cabin cooling and battery cooling simultaneously.

The cooled air from the evaporator is delivered to the cabin by a blower. Since the A/C system is kept running to regulate the evaporator at a low temperature for odor avoidance, an electric heater is utilized to warm up the cooled air and prevent cabin overcooling. The cabin air is re-circulated to the evaporator, and its rate is controlled by a re-circulation door. The modeling details of the studied TMS are discussed in the following subsections. It is noted that the unknown parameters of the control-oriented model are identified by using a high-fidelity MATLAB/Simulink® plant model that was developed based on the previous studies [35], [36] as a virtual testbed.

A. REFRIGERANT CIRCUIT MODEL

The control-oriented model of the refrigerant system is derived based on an ideal vapor-compression (VC) cycle, as shown in Fig. 2 (a). Its effectiveness was demonstrated

[1]The reheating process is enabled by the inner condenser and the positive temperature coefficient (PTC) heater.

in our previous works [30], [31], [32], [33]. This cycle describes the refrigerant at the condenser outlet and the evaporator/chiller outlet as a fully saturated liquid and a fully saturated vapor, respectively. This ideal VC cycle assumption simplifies the modeling process while still capturing the essential dynamics of the refrigerant system. The static equations for the refrigerant circuit are shown below:

$$\dot{m}_{r,comp}(h^{out}_{r,comp} - h^{out}_{r,cond}) = \dot{Q}_{cond} + \dot{Q}_{ic}, \tag{1}$$
$$\dot{m}_{r,evap}(h^{in}_{r,evap} - h^{out}_{r,evap}) = \dot{Q}_{evap}, \tag{2}$$
$$\dot{m}_{r,chlr}(h^{in}_{r,chlr} - h^{out}_{r,chlr}) = \dot{Q}_{chlr}, \tag{3}$$
$$\dot{m}_{r,comp} = \dot{m}_{r,evap} + \dot{m}_{r,chlr}, \tag{4}$$

where $h^{in}_{r,evap}$ and $h^{out}_{r,evap}$ are assumed to equal $h^{in}_{r,chlr}$ and $h^{out}_{r,chlr}$, respectively, at static conditions because of the parallel configuration. Additionally, $h^{out}_{r,cond}$ equals $h^{in}_{r,evap}$ under the adiabatic expansion valve assumption.

The specific enthalpy of the refrigerant flow at the compressor outlet, $h^{out}_{r,comp}$, is calculated by $h^{out}_{r,evap}$ and the enthalpy rise at the compressor, $\Delta h_{r,comp}$, as shown in (5). To avoid iterations by the recursive relationship with $T_{r,c}$ and $T_{r,e}$, a $\Delta h_{r,comp}$ is regressed to a function of $T_{r,c} - T_{r,e}$ under the operating range of the ideal vapor-compression cycle. The performance of the regression model is shown in Fig. 2 (b), and the equations are shown below:

$$h^{out}_{r,comp} = h^{out}_{r,evap} + \Delta h_{r,comp}, \tag{5}$$
$$\Delta h_{r,comp} = f(T_{r,c} - T_{r,e}, \dot{m}_{r,comp}). \tag{6}$$

Meanwhile, the heat transfer rates can also be formulated by the heat transfer rate at the air/coolant side with the effectiveness of the heat exchangers:

$$\dot{Q}_{ic} = \epsilon_{ic} k_{door} \dot{m}_{a,blwr} c_{p,a} (T^{out}_{r,comp} - T^{out}_{a,e}), \tag{7}$$
$$\dot{Q}_{cond} = \epsilon_{cond} \dot{m}_{a,fan} c_{p,a} (T_{r,c} - T_{amb}), \tag{8}$$
$$\dot{Q}_{evap} = \epsilon_{evap} \dot{m}_{a,blwr} c_{p,a} (T^{out}_{a,blwr} - T_{r,e}) + \dot{m}_{a,blwr} \Delta\omega h_{w,fg}, \tag{9}$$
$$\dot{Q}_{chlr} = \epsilon_{chlr} \dot{m}_{c,ewp} c_{p,c} (T^{out}_{c,bat} - T_{r,e}). \tag{10}$$

It is noted that ϵ_{evap} is evaluated based on dry air conditions to capture the sensible heat transfer rate only in the first half of (9). The latent heat transfer rate, resulting from the water condensing at the evaporator, is captured by the absolute humidity change in the second half of (9).

The air temperatures are calculated using $\dot{Q}_{ic}$ and $\dot{Q}_{evap}$ in (7) and (9), as follows:

$$T^{out}_{a,ic} = T^{out}_{a,e} + \frac{\dot{Q}_{ic}}{k_{door} \dot{m}_{r,blwr} c_{p,a}}, \tag{11}$$
$$T^{out}_{a,e} = T^{out}_{a,blwr} - \frac{\dot{Q}_{evap}}{\dot{m}_{a,blwr} c_{p,a}}, \tag{12}$$
$$T^{out}_{a,vent} = k_{door} T^{out}_{a,ic} + (1 - k_{door}) T^{out}_{a,e} + \frac{\dot{Q}_{htr}}{\dot{m}_{a,blwr} c_{p,a}}. \tag{13}$$

It should be noted that when the battery temperature is below its target temperature, the expansion valve for the chiller is closed. As a result, there is no heat transfer in the battery chiller. In this situation, the refrigerant circuit operates as a normal A/C system.

B. BATTERY COOLANT CIRCUIT MODEL

The battery coolant circuit consists of a battery pack, a battery chiller, and an electric pump for the liquid coolant.[2] In the considered working scenario, heat is generated by the battery pack and then rejected through the battery chiller to the refrigerant flow. To reduce the computational burden, the battery thermal dynamics are modeled using the lumped-mass method as follows:

$$m_{bat} c_{p,bat} \frac{dT_{bat}}{dt} = \dot{Q}_{bat} - \dot{Q}_{bat2c}, \tag{14}$$

where T_{bat} is the average temperature of the battery pack; m_{bat} and $c_{p,bat}$ are the total mass and mass-averaged heat capacity, respectively, of the battery pack, estimated based on the battery cell information. Both reversible and irreversible heat generations are considered in $\dot{Q}_{bat}$. $\dot{Q}_{bat2c}$ is the heat transfer rate from the battery to the internal coolant flow. $\dot{Q}_{bat}$ and $\dot{Q}_{bat2c}$ are expressed as follows:

$$\dot{Q}_{bat} = R_{bat} I^2_{bat} - I_{bat} T_{bat} \frac{dU_{oc}}{dT_{bat}}, \tag{15}$$
$$I_{bat} = \left(\frac{U_{oc} - \sqrt{U^2_{oc} - 4 P_{bat} R_{bat}}}{2 R_{bat}} \right) \tag{16}$$
$$\dot{Q}_{bat2c} = U_{bat} A_{bat} (T_{bat} - T_{c,eff}), \tag{17}$$
$$U_{bat} = \frac{\mathrm{Nu}_{bat} k_c}{D_{h,bat}}, \tag{18}$$
$$T_{c,eff} = \frac{1}{2} (T^{in}_{c,bat} + T^{out}_{c,bat}), \tag{19}$$

where U_{oc}, R_{bat}, and P_{bat} are the open-circuit voltage, the internal resistance, and the power of the battery, respectively; U_{bat}, k_c, and Nu_{bat} are the overall heat transfer coefficient, the thermal conductivity, and the Nusselt number of the coolant flow, respectively; A_{bat} and $D_{h,bat}$ are the surface area and the hydraulic diameter of the battery coolant channel, respectively; $T_{c,eff}$ is the effective temperature of the coolant inside the battery channel, which is calculated as the average of $T^{in}_{c,bat}$ and $T^{out}_{c,bat}$, the coolant temperature at the battery channel inlet and outlet. With $\dot{Q}_{bat2c}$ calculated with (17), the coolant temperature at the battery outlet is calculated as follows:

$$T^{out}_{c,bat} = T^{in}_{c,bat} + \frac{\dot{Q}_{bat2c}}{\dot{m}_{c,ewp} c_{p,c}}. \tag{20}$$

Given $\dot{Q}_{chlr}$, the heat transfer rate at the battery chiller is calculated with (10), the coolant temperature at the chiller outlet is calculated with a steady-state equation as follows:

$$T^{out}_{c,chlr} = T^{out}_{c,bat} + \frac{\dot{Q}_{chlr}}{\dot{m}_{c,ewp} c_{p,c}}. \tag{21}$$

[2]In the considered system, 50/50 ethylene glycol solution is used as the coolant.

The development of the state evolution prediction model based on these energy balance equations is discussed in subsection II-E.

C. CABIN MODEL

The thermal dynamics of the vehicle cabin are modeled using a lumped parameter method. The cabin air and a pseudo vehicle component, the interior structure, are treated as lumped thermal masses. The interior structure involves heat transfer with the solar radiation ($\dot{Q}_{solar}$), the ambient air convection ($\dot{Q}_{amb}$), and the interior cabin air convection ($\dot{Q}_{int}$). The lumped interior cabin air has heat transfer with the cold air from the evaporator, which is reheated before entering the cabin. The thermal dynamics of the cabin air temperature T_{cab} and the interior structure temperature T_{str} are formulated as follows:

$$\dot{T}_{cab} = \frac{1}{m_{cab}c_{p,a}}\left(\dot{Q}_{int} + \dot{m}_{a,blwr}c_{p,a}(T^{out}_{a,vent} - T_{cab})\right), \tag{22}$$

$$\dot{T}_{str} = \frac{1}{C_{str}}\left(\dot{Q}_{solar} + \dot{Q}_{amb} - \dot{Q}_{int}\right), \tag{23}$$

$$\dot{Q}_{amb} = (a_1 v_{veh} + a_2)(T_{amb} - T_{str}), \tag{24}$$

$$\dot{Q}_{int} = (a_3\dot{m}_{a,blwr} + a_4)(T_{str} - T_{cab}), \tag{25}$$

where $T^{out}_{a,vent}$ is the air temperature at the vent outlet computed by (13); T_{amb} is the ambient temperature; $\dot{Q}_{htr}$ is the heat transfer rate from the electric heater to the evaporator outlet airflow; $\dot{m}_{blwr}$ is the air mass flow rate of the blower. The mass of the cabin air, the specific heat capacity for the air, and the heat capacity of the structure are denoted by m_{cab}, $c_{p,a}$, and C_{str}, respectively, and $\dot{Q}_{amb}$ and $\dot{Q}_{int}$, which are functions of the vehicle speed v and the blower air mass flow rate $\dot{m}_{blwr}$, respectively, are calculated with the overall thermal conductance. It is noted that $\dot{Q}_{solar}$ is considered a constant value in this study.

D. POWER CONSUMPTION MODELS

In this study, three actuators in the EV TMS, which are the compressor, the fan, and the electric coolant pump, are controlled. The power consumption model of each actuator is developed and used in the cost function of the MPC to minimize the energy consumption of the TMS. On the other hand, the blower, the electric heater, and the inner condenser blend door are controlled by RB controllers instead of the MPC. This control scheme is due to the fact that the vent outlet airflow is often manually adjusted by a driver or passengers. Therefore, their power consumption is not considered in the MPC formulation.

For the development of the power consumption regression models, datasets covering a wide range of operating conditions are obtained from the high-fidelity MATLAB/Simulink® components models. The models are developed based on experimental component performance data provided by the manufacturer. These datasets include various refrigerant inlet and outlet conditions under the ideal vapor-compression cycle assumption for the compressor, the entire speed range under different vehicle speeds for the fan, and the entire speed range with different coolant temperatures for the pump.

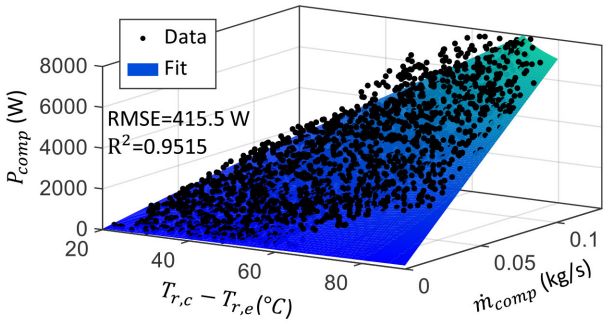

FIGURE 3. P_{comp} regression model fitted to data generated from a high fidelity compressor model.

The compressor power consumption is modeled as a static component [37]. The compressor power consumption is expressed as a function of the refrigerant temperature difference between the compressor and evaporator ($T_{r,c} - T_{r,e}$, indicating the pressure ratio) and the refrigerant mass flow rate $\dot{m}_{comp}$. It is noted that a quadratic power consumption term is highly desired for implementing quadratic programming to solve an MPC problem. The function form used in the regression model of the compressor power consumption is shown as follows:

$$\begin{aligned} P_{comp} = {} & a_{1,0}(T_{r,c} - T_{r,e}) + a_{0,1}\dot{m}_{r,comp} \\ & + a_{1,1}\dot{m}_{r,comp}(T_{r,c} - T_{r,e}) + a_{0,2}\dot{m}^2_{r,comp}, \end{aligned} \tag{26}$$

where $a_{1,0} = 1.952$, $a_{0,1} = -3813$, $a_{1,1} = 918$, and $a_{0,2} = -1.337 \times 10^4$. The overall shape of the compressor power consumption dataset is well captured by the model, as shown in Fig. 3. The root mean squared error (RMSE) is 415.5 W, and the normalized RMSE (compared with the maximum power) is 7.49%. Considering that this power consumption model is used only in the MPC, the model shows acceptable performance in obtaining an optimal energy-saving control sequence.

Similar to the compressor case, regression models to capture power consumption are developed for the fan and the electric coolant pump based on the datasets covering the entire operating range. To accommodate the implementation of quadratic programming, quadratic equation forms are used for the fan and the pump power consumption, as follows:

$$P_{fan} = \alpha_{fan}(\dot{m}_{a,fan} - \dot{m}^{lb}_{a,fan})^2, \tag{27}$$

$$P_{ewp} = \alpha_{ewp}\dot{m}^2_{c,ewp} + \beta_{ewp}\dot{m}_{c,ewp}, \tag{28}$$

where α_{fan} is a coefficient expressed as a function of vehicle speed and $\dot{m}^{lb}_{fan}$ is the lower bound of the fan airflow rate with consideration of the ram air effect, both of which are functions of vehicle speed; α_{ewp} and β_{ewp} are coefficients expressed as functions of liquid coolant temperature. Both

fan and coolant pump power consumption models show normalized RMSEs of less than 10% when compared with the dataset.

E. NONLINEAR PREDICTION MODEL FOR MPC DESIGN

Combining the equations discussed in the previous subsections, a reduced-order model of the integrated TMS is constructed in the discrete-time domain, serving as the prediction model in the proposed MPC-based controllers, which are further discussed in the following section. The reduced model comprises four state variables $x = [T_{r,c}, T_{r,e}, T_{bat}, T^{out}_{c,bat}]^T$ and three control variables $u = [\dot{m}_{comp}, \dot{m}_{fan}, \dot{m}_{c,ewp},]^T$. In the state equations for $T_{r,c}$, $T_{r,e}$, and $T^{out}_{c,bat}$, first-order filters are applied to capture any unmodeled dynamics. It is worth noting that the effectiveness of introducing a first-order filter was demonstrated in our previous work [30], [31], [32]. The state equations are then expressed as described in (29) to (32), as shown at the bottom of the next page, where k indicates the timestamp; Δt is the discretized time step; τ_{ref} is the time constant of a first-order low-pass filter applied to $T_{r,c}$ and $T_{r,e}$; τ_{bat} is the time constant of a first-order low-pass filter applied to $T^{out}_{c,bat}$ to model the thermal inertia of the coolant.

III. MPC CONTROLLER DEVELOPMENT

This section discusses the development of two controllers for the EV TMS: an economic NMPC-based controller and an LTV-MPC-based controller with an approximated value function. The steps of the controller development are covered in the following order: (i) the development of the economic NMPC controller, including the cost function and constraints, is discussed in subsection III-A; (ii) the economic NMPC controller with a long prediction horizon is considered as a baseline and tuned through a parametric study in subsection III-B; (iii) the simulation results of the baseline economic NMPC are analyzed to obtain an approximated value function in subsection III-C; and (iv) the LTV-MPC structure is developed using the approximated value function and expressed in a QP form in subsection III-D.

A. ECONOMIC NMPC-BASED CONTROLLER DESIGN

The integrated EV TMS optimal control problem is formulated as a nonlinear optimization problem, stated as follows:

$$
\begin{aligned}
\min_{u_0,\ldots,u_{Np-1}} \quad & J = \Sigma_{k=0}^{N_p-1}(P_{comp,k} + P_{fan,k} + P_{ewp,k} \\
& + w_{Taeo}(T^{out}_{a,e,k} - T^{out}_{a,e,target})^2 \\
& + w_{Tbat}\epsilon^2_{bat,k} + w_{fan}\epsilon^2_{fan,k} \\
& + w_{\Delta comp}\Delta\dot{m}^2_{comp,k} \\
& + w_{\Delta fan}\Delta\dot{m}^2_{fan,k} + w_{\Delta ewp}\Delta\dot{m}^2_{ewp,k}), \\
\text{s.t.} \quad & x_{k+1} = x_k + \Delta t \cdot f(x_k, u_k, d_k), \\
& T_{bat,k} \le T_{bat,target} + \epsilon_{bat,k}, \\
& \dot{m}^{lb}_{fan,k} - \epsilon_{fan,k} \le T_{bat,k} \le \dot{m}^{ub}_{fan,k} + \epsilon_{fan,k}, \\
& E_{zone}u_k \le F_{zone}, \\
& u^{lb}_k \le u_k \le u^{ub}_k, \\
& \Delta u^{lb}_k \le \Delta u_k \le \Delta u^{ub}_k,
\end{aligned}
$$

where J is the cost function; N_p is the number of prediction steps; $x_k = [T_{r,c,k}, T_{r,e,k}, T_{bat,k}, T^{out}_{c,bat,k}]^T$ is the system state vector; $u_k = [\dot{m}_{comp,k}, \dot{m}_{fan,k}, \dot{m}_{ewp,k}, \epsilon_{fan,k}, \epsilon_{bat,k}]^T$ is the system control input vector; Δu is the system control input increment vector; $d_k = [T_{amb}, T^{out}_{a,blwr}, \dot{m}_{blwr}, \Delta\omega, k_{door}, \dot{Q}_{htr}, v_{veh}, P_{bat}]^T$, is the disturbance vector; $f(x_k, u_k, d_k)$ is the nonlinear prediction model developed in Section II, as expressed with (29)–(32); Δt is the step size of the discrete prediction model. The inequality equations are the constraints of the state variables and control variables.

The cost function J consists of three power consumption terms, one temperature tracking term, two soft constraint terms, and three penalty terms on the control oscillations. The power consumption terms, $P_{comp,k}$, $P_{fan,k}$, and $P_{ewp,k}$, function as the economic performance costs for the economic MPC and are developed in Section II-D, as shown in (26), (27), and (28). The temperature tracking term $w_{Taeo}(T^{out}_{a,e,k} - T^{out}_{a,e,target})^2$ regulates $T^{out}_{a,e,k}$ to its target value. The two soft constraint terms, $w_{Tbat}\epsilon^2_{bat,k}$ and $w_{fan}\epsilon^2_{fan,k}$, penalize the slack variables of the soft constraints for $T_{bat,k}$ and $\dot{m}_{fan,k}$. The final three terms penalize the control variable increments to suppress oscillations. It is noted that the same cost function is used for the LTV-MPC developed in subsection III-D, which utilizes an augmented linearized prediction model using control variable increments as control inputs. Therefore, the cost terms penalizing control increments are necessary to ensure a positive definite Hessian matrix for the LTV-MPC.

The constraints of the economic NMPC include two soft constraints, a control operation zone, and the lower and upper bounds for the control variables and their increments. The battery temperature is subjected to an upper-bound soft constraint; that is, the battery is controlled below the target temperature. Considering the ram air effect by the vehicle's frontal structure, the fan's upper and lower bounds are calculated based on the vehicle speed. A soft constraint is applied to the fan's bounds to avoid numerical feasibility issues resulting from dramatic changes in vehicle speed. The control operation zone constructs linear constraints that ensure that the refrigerant system operates under the ideal vapor-compression cycle, similar to the approach used in our previous work [30], [31], [32]. A wide range of refrigerant circuit operation data is generated based on the high-fidelity MATLAB/Simulink component model. The boundaries of the operation zone are represented by five linear equations. The ideal vapor-compression cycle operation zone constraint is expressed in matrix formulation as follows:

$$
\begin{aligned}
& A_{zone}\dot{m}_{comp} + B_{zone}\dot{m}_{fan} + C_{zone}k_{door}\dot{m}_{blwr} \\
& \quad + D_{zone} \le 0
\end{aligned} \tag{33}
$$

Finally, the upper and lower bounds of the remaining control variables and their increments are applied to prevent violations of the physical limitations of the system

components. It is noted that all the constraints mentioned above are linear inequality constraints and are used in the LTV-MPC controller developed in subsection III-D.

B. A PARAMETRIC STUDY OF THE ECONOMIC NMPC

The economic NMPC controller developed in the preceding subsection has been implemented in a closed-loop simulation. The simulation results of the economic NMPC controller serve as a baseline controller for the LTV-MPC and are analyzed to obtain an approximated value function. To determine the optimal weighting factors for the economic NMPC cost function and to evaluate the performance of the economic NMPC controller, a parametric study needs to be conducted.

The outlined parametric study aims to identify the optimal combination of the weighting factors for w_{Teao} and w_{Tbat}, which affect the trade-off in temperature regulation between the refrigerant circuit and the battery coolant circuit. The simulation cases are generated by a full factorial combination of w_{Teao} and w_{Tbat}:

$$w_{Teao} \in \{10, 10^2, 2.5\times10^2, 5\times10^2, 7.5\times10^2, 1\times10^3, 10^4, 10^5\},$$
$$w_{Tbat} \in \{10, 10^2, 10^3, 10^4, 10^5\}.$$

In this study, the following parameters of the economic NMPC controller are kept constant for all simulations:

- The prediction horizon, N_p, is 500 s.
- The NMPC sampling time, Δt, is 1 s.
- The NMPC update time, Δt_{up}, is 1 s.
- The weighting factor for the slack variable on the fan bounds, α_{fan}, is 1×10^9.
- The weighting factors, $\alpha_{\Delta comp}$, $\alpha_{\Delta fan}$, and $\alpha_{\Delta ewp}$, are set at 100, resulting in relatively small values of the corresponding cost function terms compared with the power consumption and temperature tracking terms.

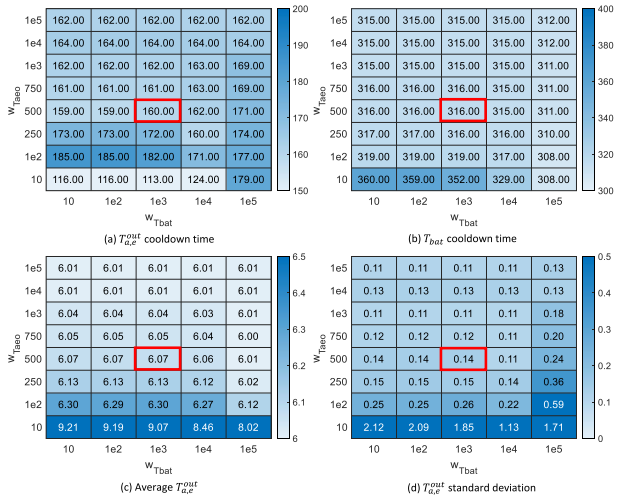

FIGURE 4. Influence of weighting factors on cooling performance with UDDS cycle at T_{amb} of 38 °C.

- $T^{out}_{a,e,target}$ is set at 6 °C to prevent unpleasant odor from the evaporator.
- $T_{bat,target}$ is set at 36 °C for the reliable and safe operation of the battery pack.

It is noted that the economic NMPC controller is configured with the longest possible prediction horizon given the computational limitations. This baseline controller serves as the basis for the approximated value function and the LTV-MPC controller. The parametric study was conducted using both the Urban Dynamometer Driving Schedule (UDDS) driving cycle and the EPA Highway Fuel Economy Test (HWFET) cycle, considering both urban and highway driving conditions. Meanwhile, the vehicle was assumed to be fully soaked at an ambient temperature of 38 °C. As mentioned in Section I, the advancement in CAV technologies enables the prediction of the ego vehicle's

$$T_{r,c,k+1} = \left(1-\frac{\Delta t}{\tau_{ref}}\right)T_{r,c,k} + \frac{\Delta t}{\tau_{ref}}\frac{1}{\epsilon_{c,k}\dot{m}_{fan,k}c_{p,a}+\dot{m}_{comp,k}a_1}\Big(\epsilon_{c,k}\dot{m}_{fan,k}c_{p,a}T_{amb}+\dot{m}_{comp,k}(h^{out}_{comp,k}-b_1) - \epsilon_{ic,k}k_{door}\dot{m}_{blwr}c_{p,a}(T^{out}_{r,comp,k}-T^{out}_{a,e,k})\Big), \tag{29}$$

$$T_{r,e,k+1} = \left(1-\frac{\Delta t}{\tau_{ref}}\right)T_{r,e,k} + \frac{\Delta t}{\tau_{ref}}\frac{1}{\epsilon_{e,k}\dot{m}_{blwr}c_{p,a}+\dot{m}_{comp,k}a_2+\epsilon_{chlr,k}\dot{m}_{c,k}c_{p,c}}\Big(\epsilon_{e,k}\dot{m}_{blwr}c_{p,a}T^{out}_{a,blwr}+\dot{m}_{comp,k}(a_1T_{r,c,k}+b_1-b_2) + \dot{m}_{blwr}\Delta\omega(a_3T^{out}_{a,e,k}+b_3)+\epsilon_{chlr,k}\dot{m}_{c,k}c_{p,c}T^{out}_{c,bat,k}\Big), \tag{30}$$

$$T_{bat,k+1} = T_{bat,k} + \frac{\Delta t}{M_{bat}c_{p,bat}}\Big(\dot{Q}_{bat,k} - U_{bat,k}A_{bat}\big(T_{bat,k}-\frac{1}{2}(T^{out}_{c,chlr,k}+T^{out}_{c,bat,k})\big)\Big), \tag{31}$$

$$T^{out}_{c,bat,k+1} = \left(1-\frac{\Delta t}{\tau_{bat}}\right)T^{out}_{c,bat,k} + \frac{\Delta t}{\tau_{bat}}\frac{1}{2\dot{m}_{c,k}c_{p,c}+U_{bat,k}A_{bat}}\Big((2\dot{m}_{c,k}c_{p,c}-U_{bat,k}A_{bat})T^{out}_{c,chlr,k}+2U_{bat,k}A_{bat}T_{bat,k}\Big), \tag{32}$$

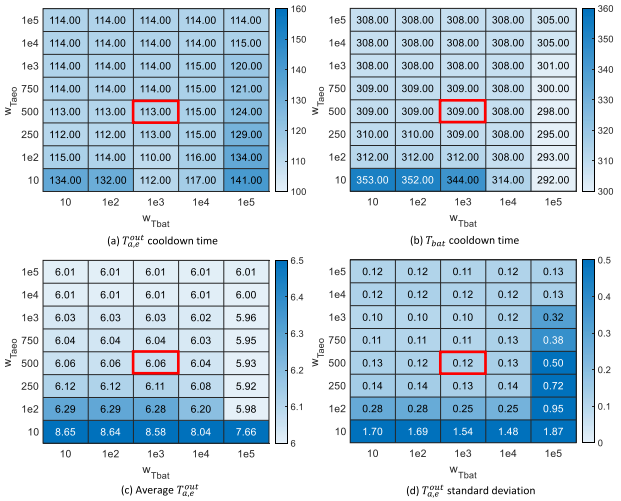

FIGURE 5. Influence of weighting factors on cooling performance with HWFET cycle at T_{amb} of 38 °C.

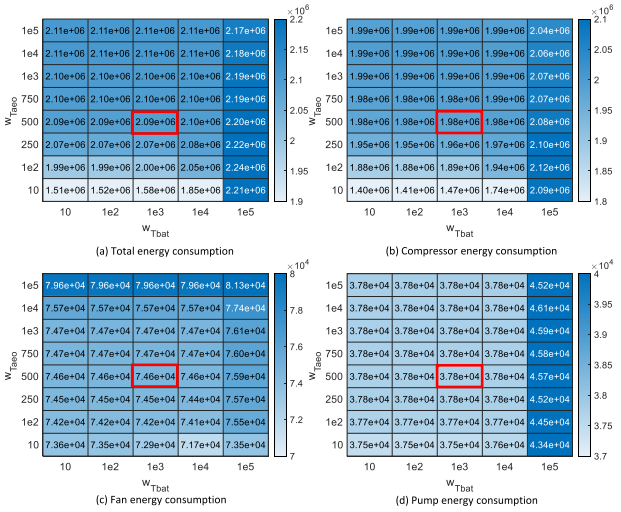

FIGURE 6. Influence of weighting factors on energy consumption with UDDS cycle at T_{amb} of 38 °C.

future speed. Therefore, this future speed profile and the corresponding battery heat generation profile of the driving cycle were assumed to be known disturbances in the MPC design. Additionally, the vehicle was assumed to start with the ambient temperature at the initial time of the simulations. For the construction of the economic NMPC controller, MPCTools [38], [39] was used, and the optimal control was solved using the nonlinear solver "Ipopt" [40] on a desktop computer with a 3.6 GHz processor.

The results of the parametric study are presented in the following heat maps. Figures 4(a)–(d) and Figures 5(a)–(d) illustrate the $T_{a,e}^{out}$ cooldown time (the time step when the $T_{a,e}^{out}$ variation is below 0.5 °C for the following 100 s), the T_{bat} cooldown time (the time step when T_{bat} reaches $T_{bat,target}$ and the expansion valve is closed), the average $T_{a,e}^{out}$ after the $T_{a,e}^{out}$ cooldown time, and the standard deviation of $T_{a,e}^{out}$ after the $T_{a,e}^{out}$ cooldown time in two driving cycles. Figures 6(a)–(d) and Figures 7(a)–(d) illustrate the total energy consumption of all three actuators. the energy

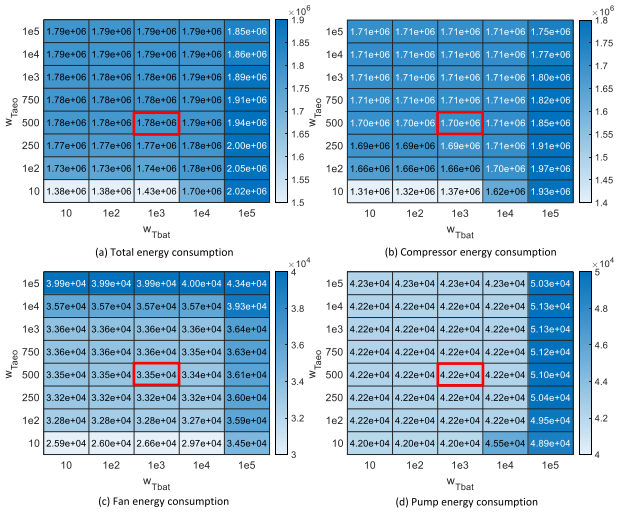

FIGURE 7. Influence of weighting factors on energy consumption with HWFET cycle at T_{amb} of 38 °C.

consumption of the compressor, the energy consumption of the fan, and the energy consumption of the coolant pump. From the heat maps, one can observe that the impact of the weighting factor combinations is similar between the two driving cycles in the cooling performance and the energy consumption.

As shown in the heat maps, a higher w_{Teao} leads to better temperature tracking performance for $T_{a,e}^{out}$, including the average $T_{a,e}^{out}$ value closer to the target and a faster $T_{a,e}^{out}$ cooldown time except for the UDDS cycle cases that have $w_{Teao} = 10$ (too small to reach the $T_{a,e}^{out}$ target). However, a higher w_{Teao} also results in higher total energy consumption due to increased usage of the compressor and fan. The standard deviation of $T_{a,e}^{out}$ does not change significantly unless w_{Teao} is too small, when $T_{a,e}^{out}$ is not adequately controlled to the target temperature. It is also observed that the usage of the coolant pump is not sensitive to the changes in w_{Teao}.

On the other hand, a higher w_{Tbat} brings a faster T_{bat} cooldown time, although the difference is not as significant as $T_{a,e}^{out}$ due to the large thermal mass of the battery pack. The faster T_{bat} cooldown time is achieved mainly by a more intense operation of the refrigerant circuit (compressor and fan operation). The coolant pump operation does not change much unless w_{Tbat} is as large as 10^5. Because of the high usage of the refrigerant circuit by large w_{Tbat}, the temperature tracking performance is also better with a larger w_{Tbat}.

In consideration of the cooling performance of $T_{a,e}^{out}$ and T_{bat}, as well as the energy consumption with the two driving cycles, the combination of $w_{Taeo} = 5 \times 10^2$ and $w_{Tbat} = 10^3$ is selected for the baseline economic NMPC. The selected combination is highlighted with a red box in the heat maps.

C. APPROXIMATED VALUE FUNCTION

In this subsection, the development of a modified approximated value function is discussed. As mentioned in Section I,

the approximated cost-to-go method, or the approximated value function, has been proven effective in solving MPC problems quickly by reducing the prediction horizon. The concept of the approximated value function is based on Bellman's principle of optimality [41], [42], [43]. In an optimal control problem, the global optimal control sequence for a given time and an initial state is solved via the following equation:

$$\min_u \Sigma_{k=t}^{t+t_f} L(x,u,d,k) = \min_u \left(\Sigma_{k=t}^{t+t_H} L(x,u,d,k) + \Sigma_{k=t+t_H+1}^{t+t_f} L(x,u,d,k) \right) \tag{34}$$

where t is the given time step; t_f is the length of the entire cycle; t_H is the length of the prediction horizon; L is the stage cost function; x, u, d, k are the state vector, control vector, disturbances vector, and the time step, respectively. According to the definition of the cost-to-go, (34) is equivalent to the following equation:

$$\min_u \left(\Sigma_{k=t}^{t+t_H} L(x,u,d,k) + V(x(t+t_H+1), t+t_H+1) \right) \tag{35}$$

where V is a function of the terminal state (with respect to the prediction horizon) and its time step (with respect to the entire cycle), which needs to consider the entire cycle. By having a value function $\hat{V}$ approximating V, the previous equation becomes a sub-optimal formulation:

$$\min_u \left(\Sigma_{k=t}^{t+t_H} L(x,u,d,k) + \hat{V}(x(t+t_H+1)) \right) \tag{36}$$

where $\hat{V}$ serves as a terminal cost term that considers only the terminal state. As a result, the computation duration is reduced from the entire cycle to the prediction horizon.

Typically, the approximated value function is developed based on the DP solution, which provides a global optimal control sequence. Park and Ahn [18] and Kibalama et al. [15] both developed data-driven functions to approximate the cost-to-go values of the DP solution in the battery-cooling-only or HVAC-only operation scenarios. While DP computation is feasible in the HVAC-only or battery-cooling-only scenarios due to the limited number of state variables, it becomes too intensive for the integrated TMS studied in this paper. Therefore, instead of the solution from DP, the solution from the economic NMPC controller with a sufficiently long prediction horizon is used, as suggested in [44].

The economic NMPC controller described in Section III-A, with the weighting factors tuned in Section III-B, was implemented in simulations with different initial conditions. In each simulation, the stage cost at each prediction step of each NMPC computation was recorded and analyzed. A total of 99 cases were considered, each with different initial battery temperatures and combinations of initial refrigerant

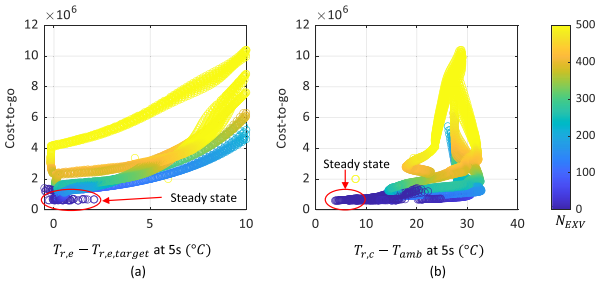

FIGURE 8. Trajectories of cost-to-go values obtained over the prediction horizon from 5 s to 500 s with respect to (a) $T_{r,e} - T_{r,e}^{target}$ and (b) $T_{r,c} - T_{amb}$ at every 5 seconds in the prediction horizon.

temperatures, as follows:

$$\begin{aligned} T_{bat,0} = T_{amb} \in \{&24, 32, 34, 36, 37, 38, 39, 40, 42\}, \\ [T_{r,c,0}, T_{r,e,0}] \in \{&[20, -10], [20, 20], [40, -10], [40, 20], \\ &[40, 40], [60, -10], [60, 20], [60, 40], \\ &[80, -10], [80, 20], [80, 40]\}. \end{aligned}$$

Based on the simulation results, a value function has been developed to approximate the cost-to-go of the economic NMPC from 5 s to 500 s in the prediction horizon. After analyzing the cost-to-go data, three variables were found to have a large impact on the cost-to-go value: $T_{r,c}$, $T_{r,e}$, and N_{EXV}, the latter representing the closing time step of the electric expansion valve to shut down the battery chiller when T_{bat} drops below its target.

Figures 8(a) and (b) show the trajectories of the cost-to-go values of the 99 cases (obtained over the prediction horizon from 5 s to 500 s) over the entire simulation with respect to $T_{r,c}$ and $T_{r,e}$, respectively, at every 5 seconds in the prediction horizon. It is observed that the cost-to-go value decreases as both $T_{r,c}$ and $T_{r,e}$ approach their steady-state temperatures. At steady state, $T_{r,c}$ has a close relationship with the ambient temperature T_{amb}, while $T_{r,e}$ reaches its target. On the other hand, the cost-to-go value decreases as N_{EXV} decreases. This is because when T_{bat} reaches its target at N_{EXV}, the cost terms associated with T_{bat} become zero for the rest of the prediction. It is important to note that, since the approximated value function cannot utilize the MPC model for long-horizon T_{bat} predictions, N_{EXV} has to be estimated by T_{bat} projections. The future trajectory of T_{bat} is first computed based on the averaged gradient derived from data stored over the past 30 seconds. The estimated closing time step, $\tilde{N}_{EXV}$, is determined as the point at which the future T_{bat} reaches the target temperature. It is noted that $\tilde{N}_{EXV}$ is limited between 0 s and 500 s, considering that the prediction horizon of the baseline economic NMPC controller is 500 s. Since N_{EXV} affects the chiller operation and subsequently $T_{r,e}$, a term involving $\tilde{N}_{EXV}$ is used as a multiplier for the $T_{r,e}$ term in the data-driven function. Additionally, this $\tilde{N}_{EXV}$-related multiplier should remain positive throughout the entire simulation. Since the approximated value function is included as a terminal cost function in a QP problem, a quadratic equation form is used. The developed data-driven

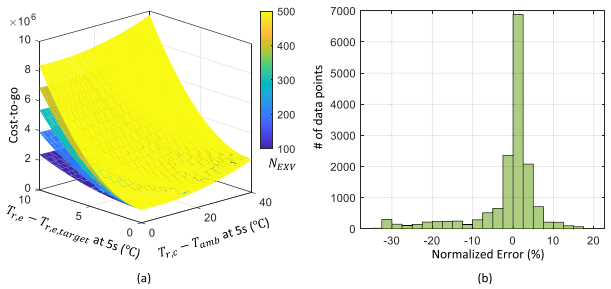

FIGURE 9. (a) the approximated value function and (b) the histogram of normalized error against collected data.

TABLE 1. Calibrated parameters of the approximated value function.

Data set	p_1	p_2	p_3	p_4
99 cases	1096	4.64	149.98	8.4925×10^5
99 cases with 44 supplemental cases	1453	4.82	145.33	7.9993×10^5

approximated value function is shown below:

$$\hat{V} = p_1(T_{r,c} - T_{amb} - p_2)^2 + p_3(\tilde{N}_{EXV} + \gamma)(T_{r,e} - T_{r,e}^{target})^2 + p_4 \quad (37)$$

where the calibrated parameters are $p_1 = 1096$, $p_2 = 4.82$, $p_3 = 149.98$, and $p_4 = 8.4925 \times 10^5$. Here, γ is introduced to ensure a positive multiplier for the $T_{r,e}$ term when $\tilde{N}_{EXV} = 0$. For simplicity, $\gamma = 1$ is used in this study. The cost-to-go value from the data-driven function (37) and its normalized error against data gathered from the simulations are presented in Fig. 9(a) and (b), respectively. The normalized error is calculated using the scale of the maximum cost-to-go value gathered in the simulations. As shown in Fig. 9 (b), the majority of the errors fall between 0 and 2.5%, indicating the effectiveness of (37) and its potential in reducing the prediction horizon.

Besides the 99 cases, an additional 44 cases were considered as supplemental simulation data to examine the impact of high initial battery temperatures under relatively low ambient temperature circumstances (e.g., the vehicle is launched after fast charging). The initial temperatures for these simulations are shown as follows:

$$\begin{aligned} &T_{amb} = 32, T_{bat,0} \in \{38, 39, 40, 42\}, \\ &[T_{r,c,0}, T_{r,e,0}] \in \{[20, -10], [20, 20], [40, -10], [40, 20], \\ &\qquad [40, 40], [60, -10], [60, 20], [60, 40], \\ &\qquad [80, -10], [80, 20], [80, 40]\}. \end{aligned}$$

The calibrated parameters of (37) using the additional data set are provided in Table 1. The error levels of both calibrations are shown to be similar. By incorporating the supplemental simulation data, the parameter p_2, which serves as the target of $T_{r,c}$, closely aligns with the parameter calibrated from the original data set. Because of the relatively higher battery cooling demand in the supplemental cases, the multipliers p_1 and p_3 need to be adjusted, but they still remain similar to the parameters derived from the original data set. This consistency in calibration denotes that the control target is not sensitive to the difference between the battery temperature and the ambient temperature, indicating that the function form in (37) possibly addresses varying initial battery temperature conditions.

D. LTV-MPC DEVELOPMENT AND ITS QP FORM

In this subsection, the development of the LTV-MPC controller is explained. The key process of the LTV-MPC development is the linearization of the nonlinear model, which will be explained in detail. As the cost function and constraints of the economic NMPC remain the same in the LTV-MPC controller, they are not covered in this subsection. The QP formulation of the LTV-MPC will be presented at the end of this subsection.

The nonlinear model discussed in Section II is linearized for the LTV-MPC. At an operating point, (x_l, u_l, d_l), in the prediction horizon, the nonlinear model is linearized as follows:

$$\begin{aligned} x_{k+1} = x_k &+ \Delta t \left.\frac{\partial f}{\partial x_k}\right|_{(x_l,u_l,d_l)} (x_k - x_l) \\ &+ \Delta t \left.\frac{\partial f}{\partial u_k}\right|_{(x_l,u_l,d_l)} (u_k - u_l) \\ &+ \Delta t \cdot f(x_l, u_l, d_l), \end{aligned} \quad (38)$$

A sequence of linearization points, $\{(x_{0,k}, u_{0,k}, d_{0,k}), \ldots, (x_{N_p-1,k}, u_{N_p-1,k}, d_{N_p-1,k})\}$, is needed when the nonlinear model is linearized by (38). The steps to obtain this sequence of linearization points are summarized as follows: (i) an estimated control trajectory for the k-th step is obtained by shifting the optimal control trajectory at the $(k-1)$-th step, $\{u_{0,k-1}, u_{1,k-1}, \ldots, u_{N_p-1,k-1}\}$, one step forward to $\{u_{1,k-1}, u_{2,k-1}, \ldots, u_{N_p-1,k-1}, u_{N_p-1,k-1}\}$; (ii) an estimated states sequence, $\{x_{1,k}, x_{2,k}, \ldots, x_{N_p,k}\}$, is obtained by applying the estimated control trajectory at the k-th step to the k-th states, $x_{0,k}$, with the nonlinear model and the updated disturbances; (iii) the estimated state sequence and the estimated control trajectory at the k-th step are combined to form the sequence of linearization points.

Since the LTV-MPC shares the same cost function and constraints with the economic NMPC, cost terms and constraints on the rate of control input are included. In the economic NMPC controller structure, the rates of the control inputs are handled by the interface of MPCTools. However, in the QP problem, the rates of the control inputs need to be included to form matrices. Therefore, the system is augmented to a velocity form by substituting u_k with $u_k = v_{k-1} + \Delta u_k$ as follows:

$$\begin{aligned} v_{k-1} &= [\dot{m}_{comp,k-1}, \dot{m}_{fan,k-1}, \dot{m}_{ewp,k-1}, 0, 0]^T, \\ \Delta u_k &= [\Delta\dot{m}_{comp,k}, \Delta\dot{m}_{fan,k}, \dot{m}_{ewp,k}, \epsilon_{fan,k}, \epsilon_{bat,k}]^T. \end{aligned} \quad (39)$$

By replacing v_{k-1} with a three-dimensional vector $v_{k-1} = [\dot{m}_{comp,k-1}, \dot{m}_{fan,k-1}, \dot{m}_{ewp,k-1}]^T$, one can eliminate the redundant 0s in v_{k-1}. Then, the linearization point (x_l, u_l, d_l)

becomes $(x_l, v_{l-1} + \Delta u_l, d_l)$, and the linearized original system is expressed as follows:

$$x_{k+1} = A_k x_k + \bar{B}_k v_{k-1} + B_k \Delta u_k + \delta_k, \tag{40}$$

with

$$\begin{aligned}
A_k &= \Delta t \left.\frac{\partial f}{\partial x_k}\right|_{(x_l,u_l,d_l)} + I_{4\times 4},\\
B_k &= \Delta t \left.\frac{\partial f}{\partial u_k}\right|_{(x_l,u_l,d_l)},\\
\bar{B}_k &= \Delta t \left.\frac{\partial f}{\partial v_k}\right|_{(x_l,v_l,d_l)},\\
\delta_k &= -\Delta t\left(\left.\frac{\partial f}{\partial u_k}\right|_{(x_l,u_l,d_l)} u_l + \left.\frac{\partial f}{\partial x_k}\right|_{(x_l,u_l,d_l)} x_l \right)\\
&\quad + \Delta t \cdot f(x_l, u_l, d_l).
\end{aligned}$$

By introducing an augmented state vector $\xi_k = [x_k, v_{k-1}]^T$, the augmented system is expressed as follows:

$$\xi_{k+1} = A_{aug,k}\xi_k + B_{aug,k}\Delta u_k + D_k, \tag{41}$$

with

$$A_{aug,k} = \begin{bmatrix} A_k & \bar{B}_k \\ 0_{3\times 3} & I_{3\times 3} \end{bmatrix}, B_{aug,k} = \begin{bmatrix} B_k \\ I_{3\times 3}\ 0_{3\times 2} \end{bmatrix}, D_k = \begin{bmatrix} \delta_k \\ 0_{3\times 1} \end{bmatrix}.$$

The linearized augmented system in (41), along with the quadratic cost function and linear inequality constraints, is assembled into the matrices to a QP problem for the LTV-MPC:

$$\begin{aligned}
\min_{\hat{U}} J &= \theta^T \tilde{Q}\theta + \mu^T \tilde{R}\mu + \tilde{q}_\xi \theta\\
&= \frac{1}{2}(\mu^T H \mu + 2q^T \mu + \hat{c}),\\
\text{s.t.} \quad & G\mu \le W + E\xi_0,
\end{aligned} \tag{42}$$

where θ and μ are the stacked state vector and control vector; the matrices $\tilde{Q}$, $\tilde{R}$, and $\tilde{q}$ are constructed with the weighting factors and parameters from the cost function. By expressing θ with μ as given by (43), the original equation is transformed into a quadratic equation in terms of μ only, with matrices H, q, and $\hat{c}$. Particularly, H is the Hessian matrix of the QP problem. Similarly, all the linear inequality constraints are stacked and expressed using μ with matrices G, W, and E. The equation to express θ with μ is given below:

$$\theta = S\mu + M\xi_0 + \Gamma\Phi, \tag{43}$$

with

$$\begin{aligned}
\theta &= \left[\xi_1\ \xi_2\ \ldots\ \xi_{N_p}\right]^T,\\
\mu &= \left[\Delta u_0\ \Delta u_1\ \ldots\ \Delta u_{N_p-1}\right]^T,\\
\Phi &= \left[D_0\ D_1\ \ldots\ D_{N_p-1}\right]^T,
\end{aligned} \tag{44}$$

where matrices S, M, and Γ are derived from the LTV prediction model in (40).

IV. SIMULATION RESULTS AND DISCUSSION

This section presents the performance of the LTV-MPC controller with the approximated value function under four driving cycles: the UDDS, the HWFET, the Worldwide Harmonized Light Vehicles Test Cycle (WLTC), and the US06 Supplemental Federal Test Procedure. It is noted that the UDDS and HWFET cycles were used to calibrate weighting factors as well as to develop the approximated value function, considering both urban and highway driving conditions. Thus, for additional performance validations, the WLTC and US06 cycles were incorporated. Specifically, the WLTC cycle was employed since it was designed to closely simulate real-road driving conditions, accommodating both low and high vehicle speed circumstances. The US06 cycle was used to supplement for aggressive driving conditions. Besides the four driving cycles, two temperature conditions were considered in the evaluation: (i) the vehicle was soaked entirely at an ambient temperature of 38 °C; (ii) the vehicle was exposed to an ambient temperature of 32 °C while the battery temperature was at 38 °C. Combining the four driving cycles and two temperature conditions, a total of eight driving conditions were considered for the controller performance evaluation. The LTV-MPC controller is compared with the baseline economic NMPC controller developed in Section III-A and an RB controller. The LTV-MPC problem is solved by using qpOASES [45]. For a fair computation time comparison between the LTV-MPC and the economic NMPC, both optimal control problems are solved on the same desktop computer with a 3.6 GHz processor.

The RB controller is responsible for controlling the compressor speed to meet the desired $T_{a,e}^{out}$. Meanwhile, the fan is controlled by a pre-calibrated rule based on the refrigerant pressure at the condenser and on the vehicle speed. The blower operation is adjusted to achieve the desired cabin cooling power in response to thermal loads. Lastly, the inner condenser vent door is controlled to adjust the vent outlet temperature and avoid excessively cold vent outlet air.

Figure 10 shows the cooling performance of three controllers under eight different driving conditions. The LTV-MPC exhibits a relatively shorter $T_{a,e}^{out}$ but a longer T_{bat} cooldown time than the economic NMPC, the differences ranging from 10 to 40 s and from 10 to 15 s, respectively. Meanwhile, the LTV-MPC demonstrates a slightly compromised average $T_{a,e}^{out}$ and a slightly higher standard deviation of $T_{a,e}^{out}$ compared with the economic NMPC. The average $T_{a,e}^{out}$ by the LTV-MPC ranges from 6.35 to 6.47 °C, deviating approximately 0.3 to 0.4 °C more from the target value than the NMPC. The $T_{a,e}^{out}$ standard deviation by the LTV-MPC is around 0.6 $\sim$ 0.88 °C, which is slightly higher than the economic NMPC results (0.5 $\sim$ 0.7 °C). The temperature tracking performance of the LTV-MPC is slightly affected by linearization and the shortened prediction horizon. However, the LTV-MPC consistently exhibits similar temperature tracking performance to the economic NMPC across all

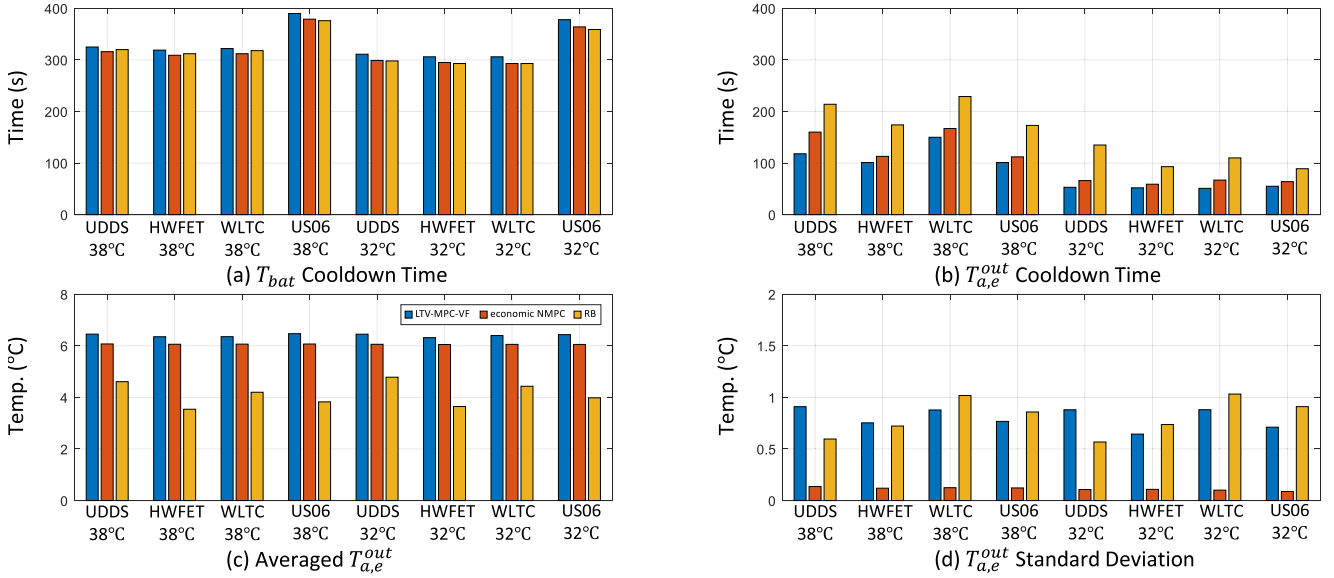

FIGURE 10. Simulation results: cooling performance of LTV-MPC-VF, economic NMPC, and RB controller at T_{amb} of 38 °C and 32 °C.

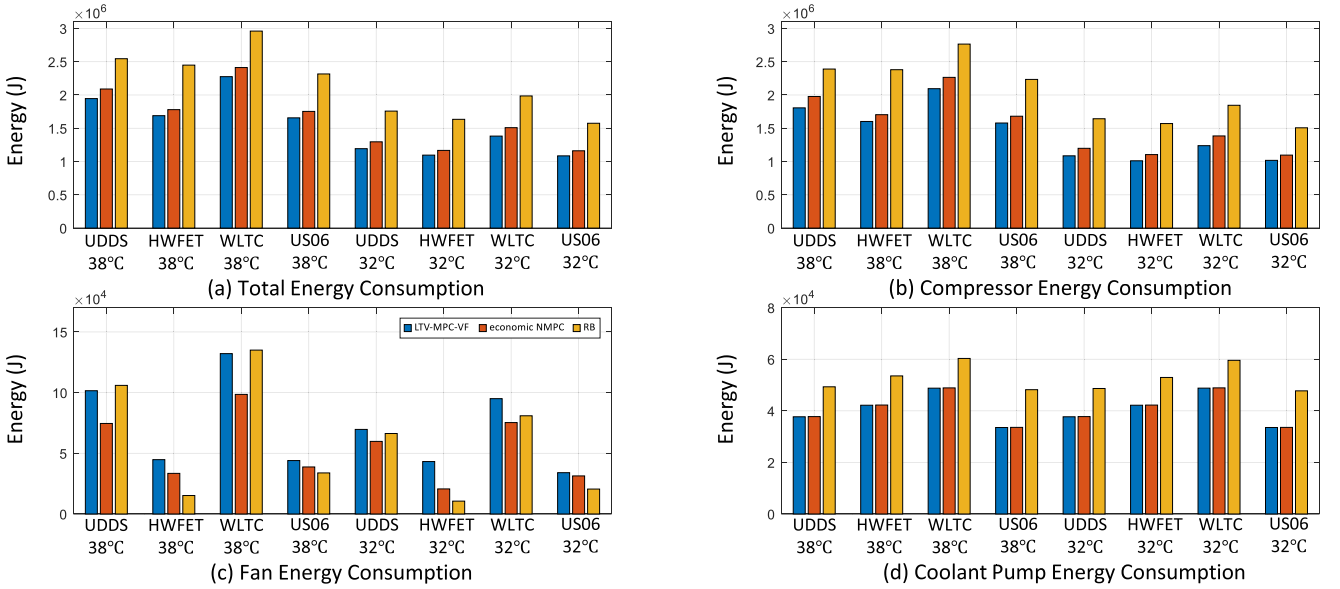

FIGURE 11. Simulation results: energy consumption of LTV-MPC-VF, economic NMPC, and RB controller at T_{amb} of 38 °C and 32 °C.

eight driving conditions, significantly outperforming the RB controller.

Figure 11 shows the energy consumption performance of the controllers under eight driving conditions. Regarding the total energy consumption of all three controlled actuators, both the LTV-MPC and the economic NMPC consistently achieve significant energy savings in all driving conditions compared with the RB controller. The LTV-MPC exhibits total energy savings ranging from 23.1% to 32.9% compared with the RB controller, and the economic NMPC achieves total energy savings of 17.9% to 27.3% compared with the RB controller. Due to the slightly compromised cooling performance, the LTV-MPC saves more energy than the economic NMPC. When comparing the energy consumption by the individual components of the two MPC controllers, it is observed that the LTV-MPC uses the compressor less but the fan more than the economic NMPC. This difference in component usage is attributed to the shortened prediction horizon of the LTV-MPC. Although the approximated value function is able to estimate the cost value over the long prediction horizon, it does not fully capture the vehicle-velocity-dependent fan operation constraints, which affects the fan operation and condenser heat transfer. Therefore, suboptimal fan operation is observed in the LTV-MPC simulations. However, the LTV-MPC and economic NMPC show very similar coolant pump energy consumption.

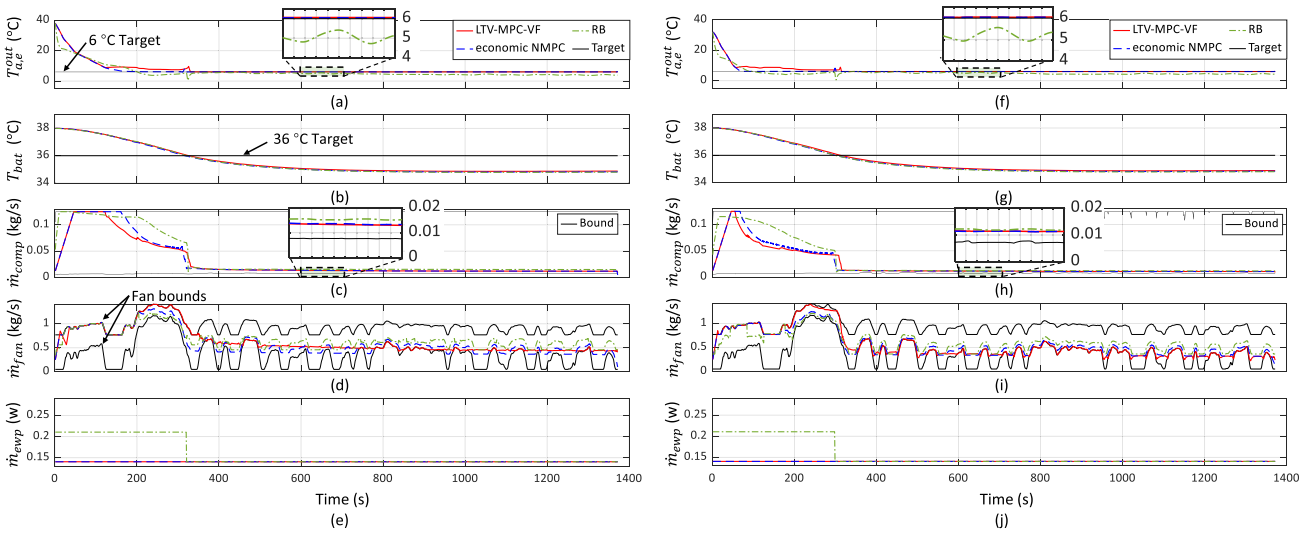

FIGURE 12. Comparison between LTV-MPC-VF, economic NMPC, and RB controller under the UDDS cycle at T_{amb} of 38 °C and 32 °C.

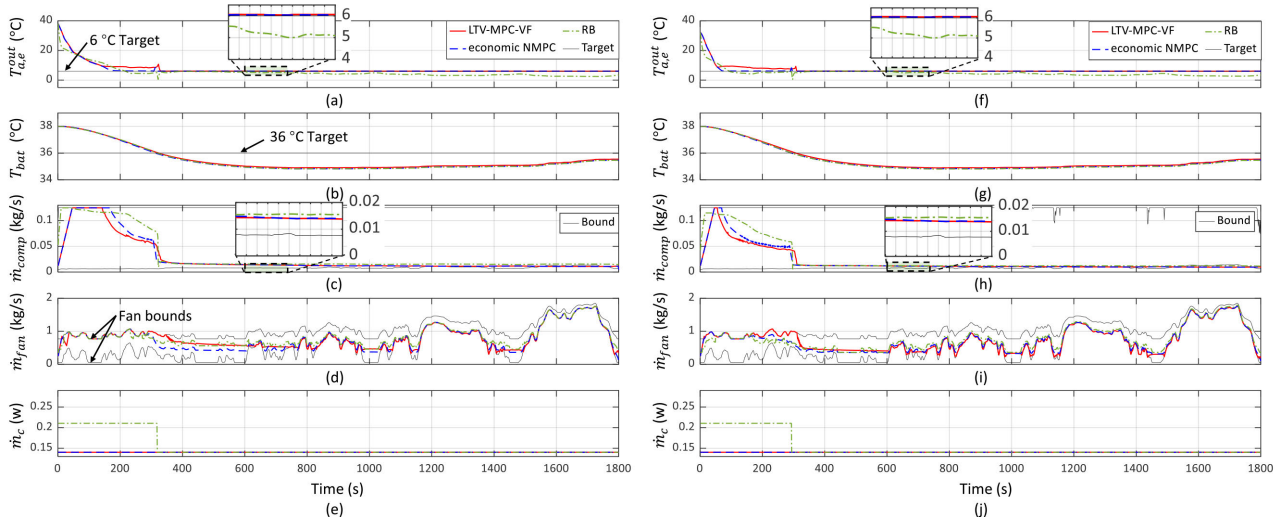

FIGURE 13. Comparison between LTV-MPC-VF, economic NMPC, and RB controller under the WLTC cycle at T_{amb} of 38 °C and 32 °C.

Figures 12 and 13 provide a comparison of the three controllers under four driving conditions as examples: the UDDS cycle with a T_{amb} of 38 °C, the UDDS cycle with a T_{amb} of 32 °C, the WLTC cycle with a T_{amb} of 38 °C, the WLTC cycle with a T_{amb} of 32 °C. Similar performance comparisons are observed under the HWFET and the US06 driving cycles. In Figures 12 and 13, the time-series trajectories of $T_{a,e}^{out}$, T_{bat}, and the three controlled actuators are presented through subplots (a)–(j). It is observed that the LTV-MPC exhibits a very similar $T_{a,e}^{out}$ trajectory to the economic NMPC. Although the LTV-MPC cools down $T_{a,e}^{out}$ to a relatively steady temperature slightly earlier than the economic NMPC, the LTV-MPC does not control the $T_{a,e}^{out}$ as close to the target as the economic NMPC does when T_{bat} has not reached $T_{bat,target}$. This is because the parameter p_2 in the approximated value function, which serves as the target of $T_{r,c}$, is calibrated with the steady state of the entire driving cycle when T_{bat} has already reached its target. However, when the battery is cooled down shortly after the evaporator, the LTV-MPC achieves a steady state $T_{a,e}^{out}$ close to the target as well as the economic NMPC does for the rest of the driving cycle. On the other hand, the RB controller experiences an overshoot of $T_{a,e}^{out}$, which leads to larger energy consumption and an oscillating steady state $T_{a,e}^{out}$ with around a 1 °C offset from the target. Regarding T_{bat}, all three controllers exhibit very similar trajectories because of the large thermal mass of the battery. The difference in T_{bat} cooldown time among the controllers is less than 10 seconds.

Because of the prediction horizon difference, the LTV-MPC shows distinct compressor and fan control trajectories. As discussed before, the approximated value function does not resolve the fan operation constraint issue caused by the short prediction horizon. Therefore, a suboptimal fan operation trajectory is observed in the

TABLE 2. Comparison of computational time of economic NMPC and LTV-MPC.

Controller	Prediction model	Prediction horizon	Computational time
Economic NMPC	Nonlinear	500 steps	5.83 s
Economic NMPC	Nonlinear	5 steps	62.73 ms
LTV-MPC	Linear	5 steps	0.58 ms

LTV-MPC. This suboptimal fan operation then affects the compressor control, especially during the first 200 s period when the compressor power demand is very high. As a result, the compromised compressor and fan control in the LTV-MPC also leads to a slightly reduced cooling performance. The coolant flow is not sensitive to the cooling performance evaluated by the selected weighting factor combination, and hence both MPC controllers refer to using the minimum allowed coolant flow. On the other hand, the RB controller, which does not consider energy consumption, tends to use the compressor more aggressively before the battery is adequately cooled down. Similarly, the coolant pump is utilized more aggressively, despite the limited battery cooling gain. Moreover, the RB controller does not account for the varying fan operation range due to vehicle speed variation, leading it to maintain a relatively steady fan duty at steady states. This, in turn, results in varying airflow at the condenser. The combination of varying air flow and slightly higher compressor operation at steady state causes an oscillating $T_{a,e}^{out}$ with an offset of around 1 °C from the target.

It is noted that a very short prediction horizon is intentionally used for the LTV-MPC in this study to evaluate the effectiveness of the method. In real practice, the cooling performance of the LTV-MPC can be further improved by utilizing a longer prediction horizon and the corresponding approximated value function based on the available computational power.

In summary, all three controllers are able to cool down the battery temperature and stabilize the evaporator air temperature at a reasonable level. However, the economic NMPC and the LTV-MPC show better performance in temperature tracking and energy saving. Comparing the two MPC controllers, it is found that the LTV-MPC has slightly compromised but similar cooling performance compared with the economic NMPC: the difference in $T_{a,e}^{out}$ cooldown time is less than 40 s; the difference in T_{bat} cooldown time is less than 15s; the difference in average $T_{a,e}^{out}$ is less than 0.4 °C; the difference in $T_{a,e}^{out}$ standard deviation is less than 0.88 °C. The overall energy-saving difference is less than 6.37%. Notably, compared with the economic NMPC, the LTV-MPC significantly improves computational performance, as presented in Table 2. This table shows that the approximated value function significantly reduces the prediction horizon, resulting in approximately 10^2 times faster computation. The linear prediction model of the LTV-MPC allows for the use of QP, which also accelerates the computation speed by a factor of 10^2. Because of these two factors, the average computation time of the LTV-MPC per MPC update can be reduced to 0.58 ms, which is much faster than that of the baseline economic NMPC, 5.83 s. In conclusion, the LTV-MPC with the approximated value function performs comparably to the economic NMPC while reducing the computation time on average by a factor of 10^4.

V. CONCLUSION

This paper proposes an MPC-based control design for an integrated TMS of an EV, including HVAC control and battery TMS control. The first step involves developing a nonlinear model of the integrated EV TMS, as described in our previous work [33]. Based on this nonlinear system model, an economic NMPC with a long prediction horizon is developed and tuned through a parametric study. For real-time implementation, a short-horizon LTV-MPC structure is developed. The prediction horizon of the LTV-MPC is reduced by introducing an approximated value function based on the long-prediction economic NMPC. As a result, the MPC computation is significantly accelerated by converting the original large-dimensional nonlinear optimization problem into a small-dimensional quadratic programming problem. The performance of the LTV-MPC with the approximated value function is evaluated against the baseline economic NMPC and the RB controller. The LTV-MPC demonstrates slightly compromised but similar cooling performance and better energy consumption compared with the baseline economic NMPC. Additionally, the LTV-MPC significantly reduces computational time by approximately 10^4 times on average, while delivering performance comparable to the baseline economic NMPC. Compared with the RB controller, the LTV-MPC controller achieves energy savings in the range of 23.1 to 32.9%.

In this work, we considered four driving cycles and two ambient temperatures in controller development and evaluation. For a more generalized and comprehensive investigation, we plan to include datasets with additional driving cycles and ambient temperatures in our future work. While a static driving environment was considered in this study, in reality, the performance of the EV TMS could be affected by complex and varying environmental conditions. Therefore, we intend in our future work to investigate the impact of variations in environmental factors such as humidity, altitude, wind speed, and solar radiation. Additionally, this study assumes that the vehicle speed profile is perfectly known. In future research, we will explore the influence of speed prediction accuracy on the control performance. Another direction for future research will involve data-driven MPC applications in a comprehensive integrated EV TMS.

ACKNOWLEDGMENT

Youyi Chen, Kyoung Hyun Kwak, Dewey Dohoy Jung, and Youngki Kim would like to acknowledge the technical support of Hyundai-Kia Motor Company.

REFERENCES

[1] Int. Energy Agency (IEA). (2023). *Global Climate Change: Vital Signs of the Planet*. [Online]. Available: https://www.iea.org/data-and-statistics/data-tools/global-ev-data-explorer

[2] D. Pevec, J. Babic, A. Carvalho, Y. Ghiassi-Farrokhfal, W. Ketter, and V. Podobnik, "A survey-based assessment of how existing and potential electric vehicle owners perceive range anxiety," *J. Cleaner Prod.*, vol. 276, Dec. 2020, Art. no. 122779.

[3] G. E. Khoury and D. Clodic, "Method of test and measurements of fuel consumption due to air conditioning operation on the new prius II hybrid vehicle," SAE, Tech. Paper 2005-01-2049, 2005.

[4] S. Bellocchi, G. Leo Guizzi, M. Manno, M. Salvatori, and A. Zaccagnini, "Reversible heat pump HVAC system with regenerative heat exchanger for electric vehicles: Analysis of its impact on driving range," *Appl. Thermal Eng.*, vol. 129, pp. 290–305, Jan. 2018.

[5] T. M. Bandhauer, S. Garimella, and T. F. Fuller, "A critical review of thermal issues in lithium-ion batteries," *J. Electrochem. Soc.*, vol. 158, no. 3, pp. R1–R25, 2011.

[6] G. Xia, L. Cao, and G. Bi, "A review on battery thermal management in electric vehicle application," *J. Power Sources*, vol. 367, pp. 90–105, Nov. 2017.

[7] E. Hyeon, J. Han, D. Shen, D. Karbowski, N. Kim, and A. Rousseau, "Potential energy saving of V2V-connected vehicles in large-scale traffic," *IFAC-PapersOnLine*, vol. 55, no. 24, pp. 78–83, 2022.

[8] T. Ard, L. Guo, J. Han, Y. Jia, A. Vahidi, and D. Karbowski, "Energy-efficient driving in connected corridors via minimum principle control: Vehicle-in-the-Loop experimental verification in mixed fleets," *IEEE Trans. Intell. Vehicles*, vol. 8, no. 2, pp. 1279–1291, Feb. 2023.

[9] X. Kong, M. A. Abdelbaky, X. Liu, and K. Y. Lee, "Stable feedback linearization-based economic MPC scheme for thermal power plant," *Energy*, vol. 268, Apr. 2023, Art. no. 126658.

[10] T. Rasku, T. Lastusilta, A. Hasan, R. Ramesh, and J. Kiviluoma, "Economic model-predictive control of building heating systems using backbone energy system modelling framework," *Buildings*, vol. 13, no. 12, p. 3089, Dec. 2023.

[11] J. A. Borja-Conde, J. M. Nadales, J. G. Ordonez, F. Fele, and D. Limon, "Efficient management of HVAC systems through coordinated operation of parallel chiller units: An economic predictive control approach," *Energy Buildings*, vol. 304, Feb. 2024, Art. no. 113879.

[12] H. Wang, M. R. Amini, Q. Hu, I. Kolmanovsky, and J. Sun, "Eco-cooling control strategy for automotive air-conditioning system: Design and experimental validation," *IEEE Trans. Control Syst. Technol.*, vol. 29, no. 6, pp. 2339–2350, Nov. 2021.

[13] H. Wang, Y. Meng, Q. Zhang, M. R. Amini, I. Kolmanovsky, J. Sun, and M. Jennings, "MPC-based precision cooling strategy (PCS) for efficient thermal management of automotive air conditioning system," in *Proc. IEEE Conf. Control Technol. Appl. (CCTA)*, Aug. 2019, pp. 573–578.

[14] J. Glos, L. Otava, and P. Václavek, "Non-linear model predictive control of cabin temperature and air quality in fully electric vehicles," *IEEE Trans. Veh. Technol.*, vol. 70, no. 2, pp. 1216–1229, Feb. 2021.

[15] D. Kibalama, Y. Liu, S. Stockar, and M. Canova, "Model predictive control for automotive climate control systems via value function approximation," *IEEE Control Syst. Lett.*, vol. 6, pp. 1820–1825, 2022.

[16] J. Lopez-Sanz, C. Ocampo-Martinez, J. Álvarez Flórez, M. Moreno-Eguilaz, R. Ruiz-Mansilla, J. Kalmus, M. Gräeber, and G. Lux, "Thermal management in plug-in hybrid electric vehicles: A real-time nmiscar model predictive control implementation," *IEEE Trans. Veh. Technol.*, vol. 66, no. 9, pp. 7751–7760, Jun. 2017.

[17] C. Zhu, F. Lu, H. Zhang, J. Sun, and C. C. Mi, "A real-time battery thermal management strategy for connected and automated hybrid electric vehicles (CAHEVs) based on iterative dynamic programming," *IEEE Trans. Veh. Technol.*, vol. 67, no. 9, pp. 8077–8084, Sep. 2018.

[18] S. Park and C. Ahn, "Model predictive control with stochastically approximated cost-to-go for battery cooling system of electric vehicles," *IEEE Trans. Veh. Technol.*, vol. 70, no. 5, pp. 4312–4323, May 2021.

[19] X. Piao, X. Wang, and K. Han, "Hierarchical model predictive control for optimization of vehicle speed and battery thermal using vehicle connectivity," *IEEE Access*, vol. 9, pp. 141378–141388, 2021.

[20] J. Glos, F. Šolc, L. Otava, and P. Václavek, "Hybrid model predictive control for fully electric vehicle thermal management system optimal mode selection," in *Proc. IECON 46th Annu. Conf. IEEE Ind. Electron. Soc.*, Oct. 2020, pp. 2036–2043.

[21] S. Zhao, M. R. Amini, J. Sun, and C. C. Mi, "A two-layer real-time optimization control strategy for integrated battery thermal management and HVAC system in connected and automated HEVs," *IEEE Trans. Veh. Technol.*, vol. 70, no. 7, pp. 6567–6576, Jul. 2021.

[22] M. R. Amini, I. Kolmanovsky, and J. Sun, "Hierarchical MPC for robust eco-cooling of connected and automated vehicles and its application to electric vehicle battery thermal management," *IEEE Trans. Control Syst. Technol.*, vol. 29, no. 1, pp. 316–328, Jan. 2021.

[23] Y. Wang and S. Boyd, "Fast model predictive control using online optimization," *IEEE Trans. Control Syst. Technol.*, vol. 18, no. 2, pp. 267–278, Mar. 2010.

[24] A. Bemporad, "A numerically stable solver for positive semidefinite quadratic programs based on nonnegative least squares," *IEEE Trans. Autom. Control*, vol. 63, no. 2, pp. 525–531, Feb. 2018.

[25] S. Schaut and O. Sawodny, "Thermal management for the cabin of a battery electric vehicle considering passengers' comfort," *IEEE Trans. Control Syst. Technol.*, vol. 28, no. 4, pp. 1476–1492, Jul. 2020.

[26] D. J. Docimo, H. C. Pangborn, and A. G. Alleyne, "Hierarchical control for electro-thermal power management of an electric vehicle powertrain," in *Proc. ASME Dyn. Syst. Control Conf.*, Sep. 2018, Art. no. V002T19A010.

[27] Y. Xie, Z. Liu, K. Li, J. Liu, Y. Zhang, D. Dan, C. Wu, P. Wang, and X. Wang, "An improved intelligent model predictive controller for cooling system of electric vehicle," *Appl. Thermal Eng.*, vol. 182, Jan. 2021, Art. no. 116084.

[28] J. Prášek, P. Trnka, V. Havlena, and P. McGahan, "Range control MPC with application to vapor compression cycles," *Control Eng. Pract.*, vol. 96, Mar. 2020, Art. no. 104309.

[29] M. Pcolka, E. Žáčeková, R. Robinett, S. Celikovskỳ, and M. Sebek, "From linear to nmiscar model predictive control of a building," *IFAC Proc. Volumes*, vol. 47, no. 3, pp. 587–592, 2014.

[30] K. H. Kwak, J. Kim, Y. Chen, Y. Kim, and D. Jung, "Economic model predictive control of HVAC system in electric vehicles," *IFAC-PapersOnLine*, vol. 54, no. 20, pp. 852–857, 2021.

[31] Y. Chen, K. H. Kwak, J. Kim, Y. Kim, and D. Jung, "Energy-efficient cabin climate control of electric vehicles using linear time-varying model predictive control," *Optim. Control Appl. Methods*, vol. 44, no. 2, pp. 773–797, Mar. 2023.

[32] K. H. Kwak, Y. Chen, J. Kim, Y. Kim, and D. D. Jung, "Thermal comfort-conscious eco-climate control for electric vehicles using model predictive control," *Control Eng. Pract.*, vol. 136, Jul. 2023, Art. no. 105527.

[33] Y. Chen, K. H. Kwak, J. Kim, D. D. Jung, and Y. Kim, "Control-oriented model of HVAC and battery cooling systems in electric vehicles," *IFAC-PapersOnLine*, vol. 55, no. 37, pp. 44–49, 2022.

[34] J. Meyer, N. Agathocleous, H. Youmans, H. Williams, T. Vespa, J. Rugh, J. Lustbader, and E. Titov, *Advanced Climate System for EV Extended Range*, document DOE-Hanon-EE0006445, 2017.

[35] J. Kim, "A study on development of simulation model and model-based predictive control algorithm for electric vehicle thermal management system," Ph.D. dissertation, Dept. of Mech. Eng., Sejong Univ., Seoul, South Korea, 2019.

[36] J. Kim, R. Rodriguez, K. H. Kwak, D. Jung, and Y. Kim, "The effect of driver's behavior and environmental conditions on thermal management of electric vehicles," SAE, Tech. Paper 2020-01-1382, 2020.

[37] T. H. Lim, Y. Shin, S. Kim, and C. Kwon, "Predictive control of car refrigeration cycle with an electric compressor," *Appl. Thermal Eng.*, vol. 127, pp. 1223–1232, Dec. 2017.

[38] J. A. E. Andersson, J. Gillis, G. Horn, J. B. Rawlings, and M. Diehl, "CasADi: A software framework for nonlinear optimization and optimal control," *Math. Program. Comput.*, vol. 11, no. 1, pp. 1–36, Mar. 2019.

[39] M. Risbeck and J. Rawlings. (2016). *MPCtools: Nmiscar Model Predictive Control Tools for Casadi*. [Online]. Available: https://bitbucket.org/rawlings-group/octave-mpctools

[40] A. Wächter and L. T. Biegler, "On the implementation of an interior-point filter line-search algorithm for large-scale nonlinear programming," *Math. Program.*, vol. 106, no. 1, pp. 25–57, Mar. 2006.

[41] D. P. Bertsekas, *Dynamic Programming and Optimal Control*. Belmont, MA, USA: Athena Scientific, 1995.

[42] H. P. Geering, *Optimal Control With Engineering Applications*. Cham, Switzerland: Springer, 2007.

[43] J. B. Rawlings, D. Q. Mayne, and M. Diehl, *Model Predictive Control: Theory, Computation, and Design*, 2nd ed. Wisconsin, CA, USA: Nob Hill Publishing, 2017.

[44] D. P. Bertsekas, *Reinforcement Learning and Optimal Control*. Belmont, MA, USA: Athena Scientific, 2019.
[45] H. J. Ferreau, C. Kirches, A. Potschka, H. G. Bock, and M. Diehl, "QpOASES: A parametric active-set algorithm for quadratic programming," *Math. Program. Comput.*, vol. 6, no. 4, pp. 327–363, Dec. 2014.

YOUYI CHEN received the B.S. degree from Xi'an Jiaotong University, Xi'an, Shaanxi, China, in 2018, and the M.S. degree in mechanical engineering from the University of Michigan–Dearborn (UM-Dearborn), Dearborn, MI, USA, in 2020, where he is currently pursuing the Ph.D. degree in mechanical engineering.

His research interests include optimization and control of vehicular systems, particularly focusing on optimal thermal management for electric vehicles.

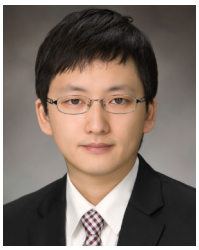

KYOUNG HYUN KWAK received the B.S. degree from Seoul National University, South Korea, in 2008, and the M.S.E. and Ph.D. degrees in mechanical engineering from the University of Michigan, Ann Arbor, MI, USA, in 2011 and 2014, respectively.

He is currently an Assistant Research Scientist with the Department of Mechanical Engineering, University of Michigan–Dearborn. His research interests include thermodynamic systems and their applications in vehicles. In particular, he is interested in looking into modeling and control of vehicle thermal and energy management systems of electric vehicles and internal combustion (IC) engines, including cabin climate control, thermal comfort, regenerative braking, cooling systems, and IC engine combustion modeling.

JAEWOONG KIM received the B.S. and M.S. degrees in automotive engineering from Ulsan University, South Korea, in 2000 and 2003, respectively, and the Ph.D. degree in mechanical engineering from Sejong University, South Korea, in 2020. He is currently with the Research and Development Division, Hyundai-Kia Motor Company, as a Global Master. Since 2003, he has been involved in researching and developing optimal control algorithms and a vehicle thermal management systems, including HVAC, PE, and HV batteries. His research interests include model-based thermal systems, the development of optimal control algorithms, and their application to software-defined vehicle.

DEWEY DOHOY JUNG received the B.S. and M.S. degrees from Seoul National University, South Korea, in 1989 and 1991, respectively, and the Ph.D. degree from the University of Michigan (Ann Arbor Campus), in 2001.

He is currently a Professor with the Mechanical Engineering Department, University of Michigan–Dearborn. He has over 30 years of academic and professional experiences in mechanical and automotive engineering. During his academic career, he has developed over 40 funded grants and contracts with an accumulated budget exceeding U.S. $4 million. Additionally, he has authored and coauthored over 60 peer-reviewed journal and conference papers. His research interests include thermal and fluid sciences and their applications to advanced energy conversion systems in automotive applications, including internal combustion engine processes and systems, hybrid/electric powertrain systems, fuel cell systems, vehicle thermal and energy management, solar energy systems, and integration, modeling, and simulation of vehicle systems.

Dr. Jung was a recipient of the Distinguished Research Award from the University of Michigan–Dearborn (2012).

YOUNGKI KIM (Senior Member, IEEE) received the B.S. and M.S. degrees from Seoul National University, South Korea, in 2001 and 2003, respectively, and the Ph.D. degree from the University of Michigan, Ann Arbor, MI, USA, in 2014, all in mechanical engineering.

He is currently an Associate Professor with the Department of Mechanical Engineering, University of Michigan–Dearborn (UM-Dearborn), Dearborn, MI, USA. Prior to joining UM-Dearborn, he held the position of a Research Engineer with Ann Arbor Technical Center, Southwest Research Institute, from 2015 to 2017. From 2003 to 2008, he was a Research Engineer with Hyundai-Kia Motor Company. His research interests include modeling and estimation/control of electrified powertrain systems, connected and automated vehicles, and energy storage systems. He was a recipient of the SAE Russell S. Springer Award (2019) from SAE International. He is an Associate Editor of IEEE TRANSACTIONS ON TRANSPORTATION ELECTRIFICATION.